# Single-pole Autoreclosure in uncompensated EHV AC mixed overhead-cable lines: a parametric time-domain analysis

A. Geri, F.M. Gatta, M. Graziani, S. Lauria, M. Maccioni

Department of Astronautics, Electrical and Energy Engineering, "Sapienza" University of Rome, Rome, Italy

## Abstract

The successful application of the Single-Pole Autoreclosure (SPAR) to Extra-High Voltage (EHV) overhead lines (OHLs), as well as to the overhead portion of EHV mixed cable-overhead lines (MLs), significantly improves system stability. SPAR success requires that the secondary arc self-extinguishes during the dead time: according to the literature, self-extinction times increase with the increase of both secondary arc current and recovery voltage. Steady-state analyses of EHV MLs not equipped with inductive shunt compensation showed larger secondary arc currents and smaller recovery voltages compared to OHLs. Since steady-state analyses cannot give indications on arc self-extinction times, transient studies are required to assess which of the above effects has a prevailing influence, i.e., whether SPAR in uncompensated MLs results hindered or facilitated. This paper presents a time-domain study of the SPAR cycle in an uncompensated 400 kV-50 Hz ML, making use of detailed ATP-EMTP line and fault arc models. A parametric study has been carried out, evaluating secondary arc current, extinction time and recovery voltage for different single-phase fault locations along the overhead section of the line. Transient simulation results point out to extinction times being shorter in MLs than in OHLs of the same total length.

Index Terms— Mixed lines, Single-Pole Autoreclosure, Secondary arc, Electromagnetic transient simulation

## 1 Introduction

A mixed line (ML) consists of solidly series-connected underground cable (CL) and overhead line (OHL) sections. At transmission level, the recourse to a ML structure might circumvent local opposition to the

construction of a new OHL [1], [2], by "undergrounding" the critical portion of the line [3]. The vast majority of ML faults occur in the OHL sections: moreover, at Extra-High Voltage (EHV) level at least 80% of OHL faults are single-phase-to-ground (1LG), and mostly transient [4]-[6]. ML relaying schemes that can reliably identify faults occurring in the overhead section [7]-[10] enable the application of Single-Pole Autoreclosure (SPAR) to such faults, improving system stability and continuity of service. Given the correct fault selection, the success of SPAR ultimately requires the definitive self-extinction of the secondary arc during the autoreclosure dead time [11], [12]. Power frequency studies of the arc current and of the subsequent recovery voltage [13], [14] evidence the role of capacitive and inductive coupling. Empirical self-extinction criteria. based on linear analyses do not take into account the non-linear, stochastic nature of the secondary arc: the actual duration of the arc and its possible extinction are very difficult to predict since a number of random factors, such as atmospheric conditions and arc elongation, come into play. This has prompted many experimental studies, including full-scale laboratory tests [5], [15]-[18] and actual staged faults at EHV and Ultra-High Voltage (UHV) level [19]-[24]. In order to arrive at credible envelopes for extinction time, SPAR time-domain simulations have to include dynamic modeling of the arc as a nonlinear time-varying resistance, based on the theory of constrained switching arc in circuit breakers [25]. A deterministic model of both the primary and secondary arc in air, represented by a dynamic arc conductance taking into account the thermal behavior of the arc column, was proposed in [26]. Alternatively, a dielectric condition could be considered to simulate arc extinction, by comparing recovery voltage with re-ignition voltage, allowing the representation of multiple re-ignitions [27]. Such models yield current and voltage waveforms with a close qualitative resemblance to actual field measurements. Subsequent refinements took into account the non-monotonic increase of the equivalent arc length, i.e., the sudden shortening due to the partial collapse of the arc [28], [29].

The vast body of research devoted to SPAR-related problems has been obviously centered on long EHV and UHV overhead lines, which are usually provided with shunt compensation [30]-[39]; very few contributions deal with the issue of secondary arcs and SPAR in EHV MLs [40], [41], [42]. In particular, [42] showed the increase of secondary arc current and the risk of harmonic resonance in a 400 kV-50 Hz ML, whereas [41] presented the transient simulation of a ML SPAR cycle. In [40] the authors estimated steady-state values of the secondary arc current and the recovery voltage of several 400 kV – 50 Hz MLs characterized by relatively short cable sections, which comply with the rated line-charging breaking current of IEC standard line circuit

breakers without need of inductive shunt compensation. The power frequency analysis, carried out on detailed multiconductor models, showed that the presence of the cable stretch has a significant impact on the line behavior during SPAR cycles. For some combinations of fault location and pre-fault line loading the secondary arc current in a ML can be substantially larger than in an all-overhead line, whereas recovery voltages are generally smaller. Notably, secondary arc currents up to 60 A RMS were calculated, whereas a commonly accepted empirical self-extinction threshold at 400 kV – 50 Hz is 40 A RMS for a 1 s dead-time [5]. In principle, an arc current increase and a recovery voltage decrease have opposite effects on arc self-extinction: steady-state, linear analyses cannot take into account the time-varying, non-linear arc behavior, so that detailed transient analyses are required to evaluate the possible self-extinction of the arc and ultimately the success of SPAR.

None of the previous works [40],[41],[42] presented a systematic transient analysis of ML SPAR. This paper presents a parametric time-domain ATP-EMTP study of SPAR application in a 201.1 km long, 400 kV-50 Hz ML, with the aim of assessing secondary arc extinction times. We chose the ML configuration with 194.4 km of OHL and 6.7 km of CL, because it was the worst case, i.e., the one which yielded the largest secondary arc currents and recovery voltages among the limit case MLs operable without inductive shunt compensation in [38]. In order to evaluate secondary arc self-extinction, a dynamic arc model [26] has been used. The time-domain parametric study is carried out varying the fault position, the pre-fault line loading and the OH ground wires composition besides the secondary arc elongation speed, to evaluate the secondary arc duration up to the self-extinction. Results are compared to those obtained for an all-overhead line of equal (201.1 km) length.

The paper is structured as follows: Section 2 recalls power frequency estimates of the inductive and capacitive secondary arc and recovery voltage components, Section 3 describes the system under study (including the arc model) and its implementation in ATP-EMTP. Transient simulation results are reported in Section 4, conclusions are presented in Section 5.

## 2 Power frequency analysis

The power frequency study in [40] was based on detailed multiconductor circuit modeling of both the overhead and cable portions of the ML, which were represented down to each CL minor section and OH tower span.

The model included ground wires, tower footing resistances, cable sheaths and their grounding resistances. Results evidenced two main peculiarities of the uncompensated ML:

- the secondary arc current can be substantially larger than in an overhead line of the same total length and having the same construction of the OH portion of the ML, in particular when the 1LG fault occurs near the overhead terminal of the ML in conjunction with a high pre-fault line loading;
- on the other hand, in case of secondary arc self-extinction the attendant recovery voltage is generally lower in the uncompensated ML.

Such behavior can be readily interpreted in terms of the simple equivalent circuits representing the capacitive and inductive coupling between the open faulted phase and the sound, energized ones. At EHV level the capacitive coupling is usually prevalent, inductive effects being of interest only for long, heavily loaded lines, and then only when the 1LG fault is located in the vicinity of the line terminals.

The capacitive components of the secondary arc current $\bar{I}_{SC}$, and recovery voltage $\bar{E}_{rc}$, can be evaluated by means of the simple equivalent circuit of Fig. 1, where $C_{oCL}$ is the cable zero-sequence capacitance, $C_{oOH}$: is the overhead line zero-sequence capacitance and $C_{mOH}$: is the overhead line interphase capacitance. The series impedance of the faulted phase and the equivalent arc resistance are neglected. The resulting expression for $\bar{I}_{SC}$ is:

$$\bar{I}_{sc} = -j\omega C_{mOH}\bar{E}_A \tag{1}$$

The capacitive current practically depends on the overhead line length only and is not influenced by the fault location. The capacitive recovery voltage is given by:

$$\bar{E}_{rc} = -\bar{E}_A \frac{C_{mOH}}{(C_{0CL}+C_{0OH})+2C_{mOH}} \tag{2}$$

For the same total length, both $\bar{I}_{sc}$ and $\bar{E}_{rc}$ will be slightly smaller for the ML, which has a smaller aggregate interphase capacitance and a significantly larger capacitance to ground than the OHL.
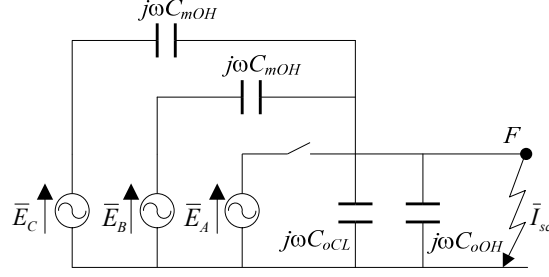
*Fig. 1 Simplified equivalent circuit (from [40]) for the evaluation of 'capacitive' secondary arc current ($I_{sc}$) and recovery voltage. F: fault location.*

The inductive current $\bar{I}_{sm}$ and recovery voltage components can be evaluated by means of the circuit of Fig. 2, which explicitly refers to a fault along the OHL section of an uncompensated ML, where $\dot{z}_s$, $\dot{z}_m$ are the 'self' and 'mutual' (interphase) impedances per unit length (p.u.l.) and $c_S = (c_0 + 2c_m)$ is the 'self' capacitance p.u.l.. Suffixes OH and CL stand for Overhead Line and Cable Line, respectively; $l_f$ is the distance to the fault. Since the Thévenin impedance seen at fault location is dominated by the shunt capacitance of the line, the CL series branch in Fig. 2 can be omitted to arrive at the approximate formulation

$$\bar{I}_{sm} \cong \left[ \frac{\dot{z}_{mOH} l_f}{\dot{z}_{sOH} l_f + \dfrac{1}{j\omega\left(c_{sCL} l_{CL} + c_{sOH}\left(\frac{l_f}{2}\right)\right)}} - \frac{\dot{z}_{mOH}(l_{OH} - l_f)}{\dot{z}_{sOH}(l_{OH} - l_f) + \dfrac{2}{j\omega\left(c_{sOH}(l_{OH} - l_f)\right)}} \right] \bar{I}_i \tag{3}$$

$\bar{I}_i$ is the inducing current, estimated as:

$$\bar{I}_i \cong -\frac{3(\bar{E}_{Th,S} - \bar{E}_{Th,R})}{2\dot{Z}_0 + \dot{Z}_1} \tag{4}$$

where $\bar{E}_{Th,S}$ and $\bar{E}_{Th,R}$ are equivalent Thévenin voltages behind the $Z_s$ and $Z_R$ source impedances at the sending and receiving end in Fig. 3, $\dot{Z}_0$ and $\dot{Z}_1$ are the zero- and positive-sequence series impedances of the overall system. The inducing current (4) basically increases with the phase displacement between source voltages, i.e., with the pre-fault line loading. For the same $\bar{I}_i$ value, the "inductive" secondary arc current component is larger for the ML than for the OHL due to the larger capacitance to ground of the ML which allows the circulation of a greater current. Moreover, when ML faults occur towards the overhead terminal, the larger ML shunt capacitance results in a higher $I_{sm}$ value. The power frequency, parametric study of the 400 kV – 50 Hz ML

in [1] evidenced an increase in the secondary arc current magnitude up to 50% compared to the all-overhead cases, with RMS values greater than 50-60 A for a 200 km-long line.
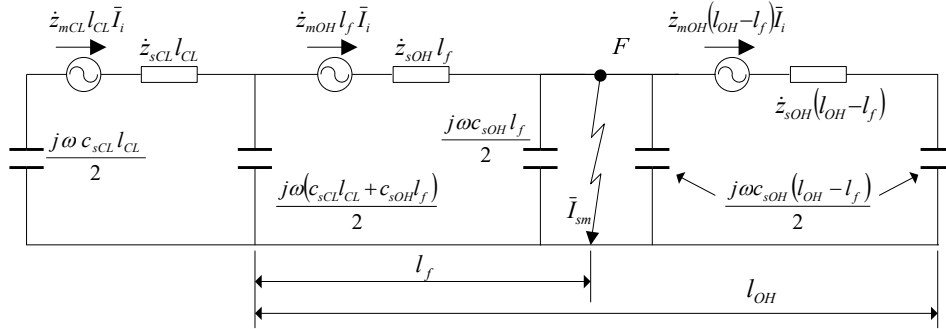


*Fig. 2 Simplified, single-phase equivalent circuit of the ML (from [40]) for the evaluation of the 'inductive' secondary arc current ($\bar{I}_{sm}$) and recovery voltage.*

The total secondary arc current is the vector sum of the capacitive and inductive components.

$$\bar{I}_s = \bar{I}_{sc} + \bar{I}_{sm} \tag{5}$$

Circuit analysis also shows that both the capacitive and inductive recovery voltage components decrease when a short cable stretch replaces the terminal portion of the overhead line.

# 3 The system analyzed

The line under study is a 400kV - 50Hz, 201.1 km long uncompensated cable-overhead mixed line consisting of a short (6.7 km) single-circuit CL stretch in series with a much longer (194.4 km) single-circuit OHL section, i.e., Case #3 of [40]. As anticipated in the introduction, this configuration was chosen as a worst-case non-compensated ML, in terms of secondary arc current and recovery voltage. The OHL portion is a typical italian 400 kV–50 Hz line construction, with triple-bundled 31.5 mm ACSR conductors in an untransposed horizontal arrangement, and two ground wires. The single-circuit CL is made of three single-core, 2500 mm$^2$ Cu, XLPE-insulated underground cables, in horizontal laying; the CL stretch is transposed with the sheaths connected in sectionalized cross-bonding. By way of comparison, all simulations have been repeated for a 201.1 km long OHL, having the same construction of the overhead portion of the ML.

The study has been carried out by means of ATP-EMTP. The OHL sections have been represented by 486 cascaded multiconductor nominal-pi circuits (type 1, 2, 3…), each one accounting for a single span of the

overhead line (5 equivalent conductors, 400 m length); shield wires are connected to the tower grounding resistances at each junction. Two different types of conductors have been considered for the ground wires of both the OH stretch of the ML and the 200 km OHL: i.e., 17.5 mm ACSR or 11.5 mm galvanized steel. The CL section has been simulated by 12 cascaded (6-conductor) pi-circuits, representing the individual 556 m long minor sections of the cross-bonded cable. CL sheaths are connected to grounding resistances at each cross-bonding major sections, and at the overhead-cable transition compound. At the line terminals, OHL ground wires and CL sheaths are connected to substation grounding resistances. The following values have been used for the different grounding resistances:

- Line terminals (substations): 1 $\Omega$

- CL - OHL transition compound: 5 $\Omega$

- CL sheaths, at the major cross-bonding sections: 25 $\Omega$

- OHL towers: 15 $\Omega$

Table 1 reports the average positive and zero-sequence p.u.l. impedances of the OHL and CL stretches evaluated by means of the ATP-EMTP LINE CONSTANTS and CABLE PARAMETERS supporting routines, which were used in the steady-state, circuit-based calculation. The relevant files are included as supplementary material.

At both terminals, the simulated line is connected to fundamental frequency (Thévenin) system equivalents with 8000 MVA short-circuit capacity and $X_0 = X_1$. Two pre-fault line loading conditions have been imposed: a 400 MW "low loading" scenario or a 1200 MW "high loading" scenario. The 1200 MW scenario is a worst case in the sense that cable current is very close to ampacity; by contrast the 400 MW scenario is an arbitrary chosen "low load" condition. With reference to Fig. 3, the direction of active power flow has been taken from bus 2 to bus 1, i.e., from the overhead terminal of the ML to the cable one; this flow direction results in larger secondary arc currents when the fault is applied near bus 2, i.e., the sending end of the line. Being associated to the magnetically induced component of the arc current, this behavior is more noticeable at high pre-fault loading. For the sake of consistency, the same power flow direction has been assumed in the overhead-only simulations. For every line configuration, 1LG faults have been simulated at 7 different locations along the

OHL, approximately spaced 32 km from each other in order to span the whole overhead sections of the ML.

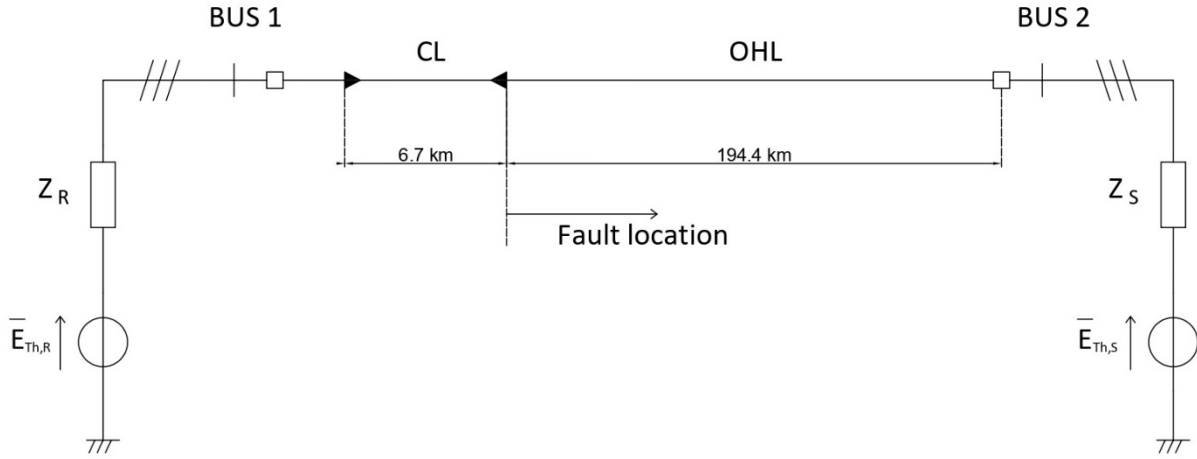The faults were applied to the most unfavorable phase of the ML.



*Fig. 3 One-line diagram of the simulated mixed line. $\bar{E}_{Th,R} = \frac{408.1}{\sqrt{3}}$ kV, $\bar{E}_{Th,S} = \frac{420}{\sqrt{3}} e^{j\theta}$ kV ($\theta = 12°$ for the 400 MW case, $\theta = 40.54°$ for the 1200 MW case).*

*Table 1 400 kV – 50 Hz OHL and CL data.*

| Type | Sequence | $r$ (Ω/km) | $x^a$ (Ω/km) | $c$ (nF/km) | $I_z^e$ (A) |
|------|----------|-----------|-----------|-----------|-----------|
| OHL[b] | Positive | 0.020 | 0.269 | 13.5 | 2700 |
|  | Zero |  |  |  |  |
|  | 1 | 0.158 | 0.684 | 8.1 |  |
|  | 2 | 0.303 | 1.022 |  |  |
| CL | Positive | 0.0137 | 0.172 | 240 | 1788 |
|  | Zero[d] |  |  |  |  |
|  | 16.7 km | 0.376 | 0.141 |  |  |
|  | 13.3 km | 0.446 | 0.182 | 240 |  |
|  | 6.7 km | 0.687 | 0.435 |  |  |

[a] reactance at 50 Hz
[b] Two shield wires, 15 Ω tower earthing resistance. (1): ɸ = 17.5 mm ACSR; (2): ɸ = 11.5 mm galvanized steel.
[c] Horizontal laying (0.35 m spacing, 1.5 m depth), 1.0 K/Wm soil.
[d] Depends on CL length and sheath earthing resistances (1 Ω terminal stations, 25 Ω major sections).
[e] Current at thermal limit.

The fault is assumed to occur between phase conductor and tower and is represented by a Kizilcay dynamic arc model [26] in ATP, (model parameters [28] are reported in Table 2).

The time-varying arc conductance $g$ is obtained from the differential equation:

$$\frac{dg}{dt} = \frac{1}{\tau}(G - g) \qquad (6)$$

where $\tau$ is the arc time constant, $g$ is the instantaneous arc conductance and $G$ is the stationary arc conductance. $G$ is defined by:

$$G = \frac{|i_{arc}|}{u_{st}} \qquad (7)$$

with

$$u_{st} = (u_0' + r_0'|i_{arc}|) \cdot l_{arc}(t) \qquad (8)$$

where $i_{arc}$ is the instantaneous arc current, $u_{st}$ is the stationary arc voltage, $l_{arc}$ is the instantaneous arc length, $u_0'$ is the characteristic arc voltage per length and $r_0'$ is the characteristic arc resistance per length. The arc time constant $\tau$ depends on the instantaneous arc length as:

$$\tau = \tau_0 \cdot \left(\frac{l_{arc}}{l_0}\right)^\alpha \qquad (9)$$

where $\tau_o$ is the initial time constant, $l_0$ is the initial arc length and $\alpha$ is a coefficient of negative value. Conditions for arc self-extinction are taken from [28]:

$$g'_{min}=50 \ \mu S \ m \qquad \text{and} \qquad \frac{dr'_{arc}}{dt} = 20 \ \frac{M\Omega}{s \cdot m} \qquad (10)$$

where $g'_{min}=1/r'$ is the arc conductance per unit length at the considered instant.

*Table 2 Arc parameters used in the Kizilcay model [28].*

| | | |
|---|---|---|
| Exponential coefficient | $\alpha$ | -0.5 |
| Initial time constant | $\tau_0$ (ms) | 1 |
| Initial arc length | $L_0$ (m) | 3 |
| characteristic arc voltage | $u_0$ (kV/m) | 0.9 |
| characteristic arc resistance | $r_0'$ (m$\Omega$/m) | 22 |

The arc model is implemented in the MODELS programming language [30] and is embodied in the time-domain simulation by means of a type-91 non-linear resistance and a type-13 controlled switch, as shown in Fig. 4.
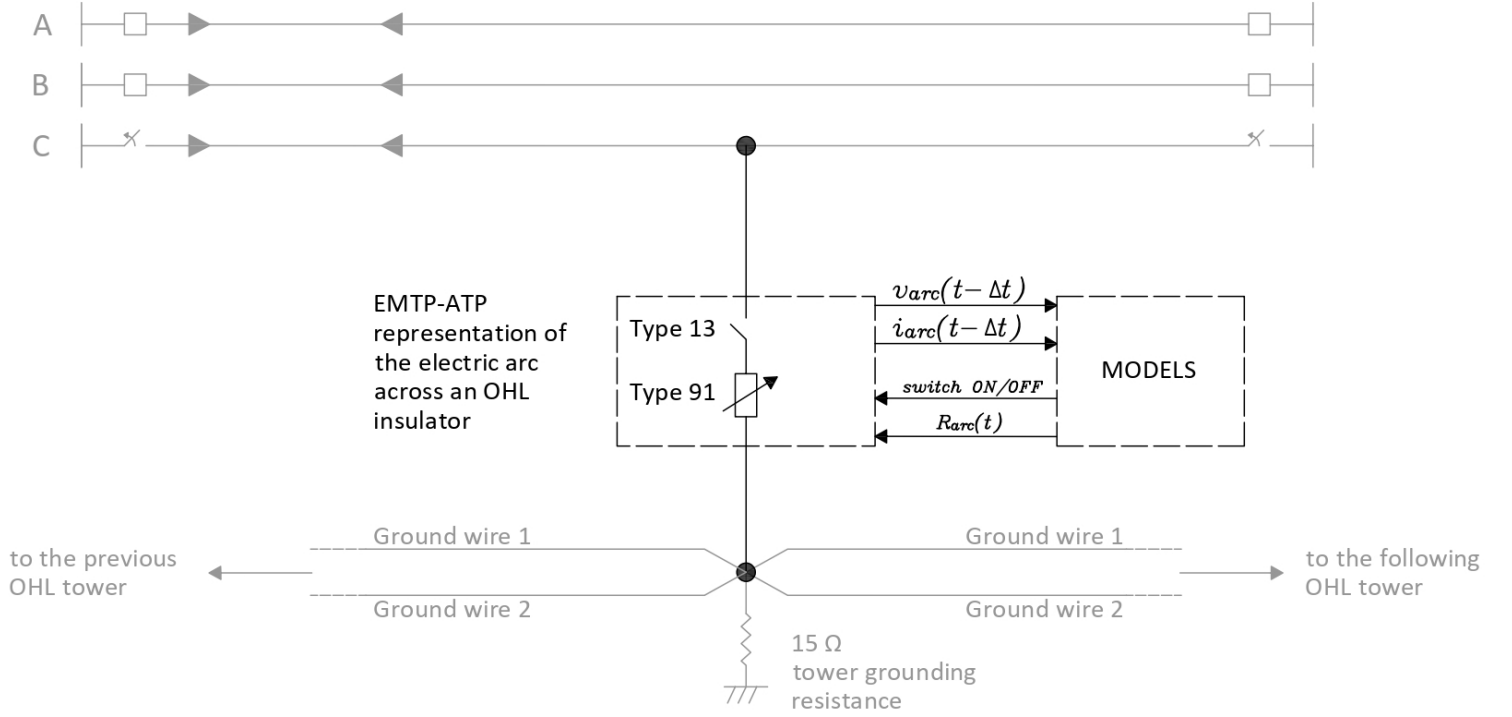


Fig. 4 Schematic diagram representing arc implementation in MODELS.

# 4 Results

## 4.1 Dynamic arc characteristics

ATP-EMTP simulations were carried out by applying the 1LG fault at $t$=0 s, single-pole tripping of the faulted phase at both line terminals followed at $t$=0.1 s. At each simulation time-step the arc conductance value is updated using arc voltage and current values from the preceding step. Initial arc length is set at $L_0$=3 m and stays constant at this value for the duration of the primary arc.

The time plot of dynamic arc resistance associated with the primary arc current, reported in Fig. 5, is quite similar for all simulated cases: the resistance oscillates between 0.4 $\Omega$ and 1.2 $\Omega$ until the faulted phase is switched off at 0.1 s determining a rapid resistance increase. After the single-pole tripping, the arc length is assumed to increase linearly with time. A wide range of values has been proposed for the simulated secondary arc elongation speed, up to 90-120 m/s. Several papers report values around 40-50 m/s. As this paper focuses

on the assessment of self-extinction, two conservatively low elongation speeds have been simulated, namely 30 m/s and an extremely low 10 m/s. On the other hand, the arc length is assumed to increase monotonically without the sudden reversals due to partial arc collapse, shown in [28] and [29].
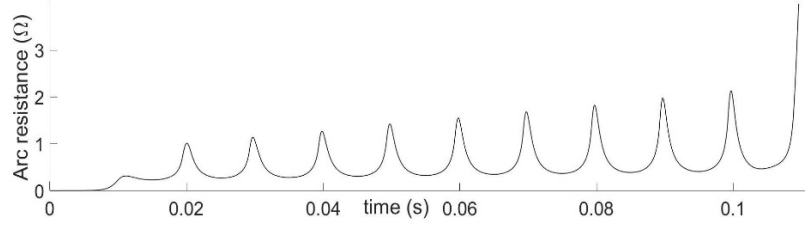


*Fig. 5 Resistance associated with the primary arc fault current vs. time. (Mixed line, steel ground wires, 1200 MW pre-fault loading, fault simulated at x = 193.9 km.).*

Pairs of voltage and current values can be plotted against each other over one cycle at power frequency, to obtain arc volt-ampere characteristics, several of which are plotted in Fig. 6. The *v-i* loci of Fig. 6 refer to different instants along the simulated existence interval of the secondary arc (first, "intermediate" and last cycle). The progressive expansion of the arc *v-i* envelopes is clearly seen.
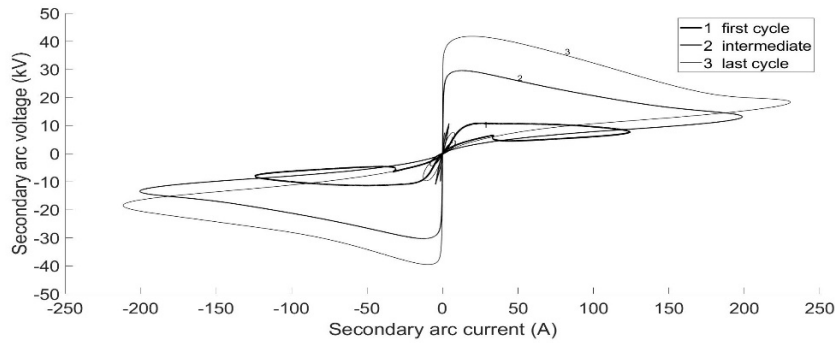


*Fig. 6 Arc dynamic Volt-Ampere characteristics for various cycles during arc persistence. (Mixed line, steel ground wires, 1200 MW pre-fault loading, $v_{arc} = 30$ m/s, fault simulated at x = 193.9 km.)*

The time plot of the secondary arc dynamic resistance for a sample case is shown in Fig. 7, evidencing the progressive increase of the peak resistance value as the arc lengthens until final extinction (after arc self-extinction, the plot stays constant at the last recorded value). This is a direct consequence of having assumed the arc length to be constant during the primary arc period and linearly increasing during the persistence of the secondary arc [15].
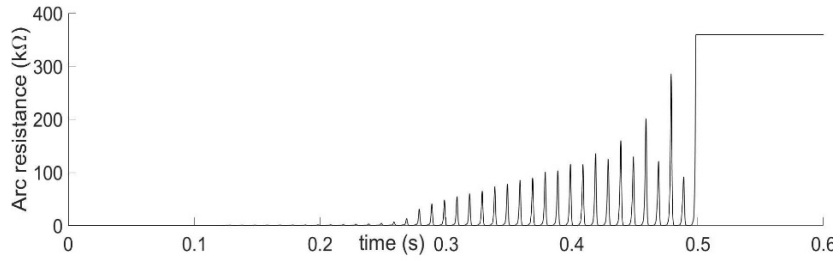
*Fig. 7 Resistance associated with the secondary arc current vs. time. (Mixed line, steel ground wires, 1200 MW pre-fault loading, $v_{arc}$ = 30 m/s, fault simulated at x = 193.9 km.)*

## 4.2 Secondary arc current

As a first step, all simulated secondary arc current waveforms have been processed in order to assess their harmonic content. In particular the power frequency components, evaluated in the first cycle after the trip of the faulted phase, have been compared to the values predicted by the circuit-based steady-state calculation of [40]. By way of example, curves of fundamental frequency RMS current are plotted in Fig. 8 as a function of the fault location along the overhead portion of the ML, for several pre-fault load/shield wire combinations.
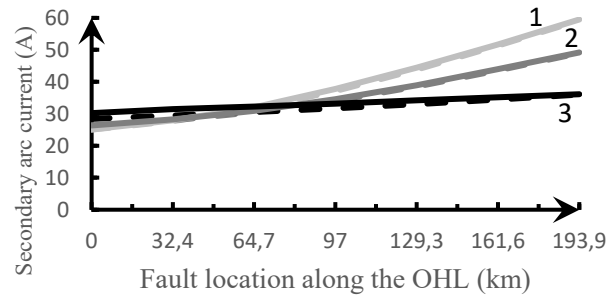


*Fig. 8 RMS power-frequency component of the secondary arc current as a function of fault location. Solid lines: ATP-EMTP simulations (in the first cycle after single-pole tripping). Dotted lines: phasor model from [40].1) Mixed line, galvanized steel shield wires (SW), 1200 MW pre-fault line loading, 2) mixed line, ACSR SW, 1200 MW pre-fault line loading, 3) mixed line, galvanized steel SW, 400 MW pre-fault line loading.*

Curves in Fig. 8 evidence a very good agreement between the linear phasor solution and the initial value of the power frequency component. Detailed time-domain simulations thus fully confirm predictions from [40], such as the secondary arc current increase in MLs with heavy pre-fault power flows, and the compounding effect of higher shield wires resistance. Since the arc length is assumed to increase linearly with time after the

faulted phase is tripped, arc current and voltage waveforms also change with time: by way of example, Fig. 9 and Fig. 10 respectively show the simulated ML secondary arc current and voltage waveforms for the case of steel ground wires, 1200 MW pre-fault power, $v_{arc}$ = 30 m/s, fault at $x$=193.9 km along the OH line section.

In this particular case, the arc self-extinguishes around t = 0.5 s. Fig. 9 and Fig. 10 clearly show that at the beginning of the secondary arcing period waveforms are dominated by the power frequency component, with a relatively small harmonic content. The arc non-linearity results in increasingly distorted waveforms as the secondary arc lengthens. This is exemplified by Fig. 11, which shows secondary arc current harmonic spectra evaluated in the first cycle after pole tripping and in the last cycle prior to arc extinction, for another sample case (fault at $x$=129.3 km, ACSR shield wires and 1200 MW pre-fault line loading).
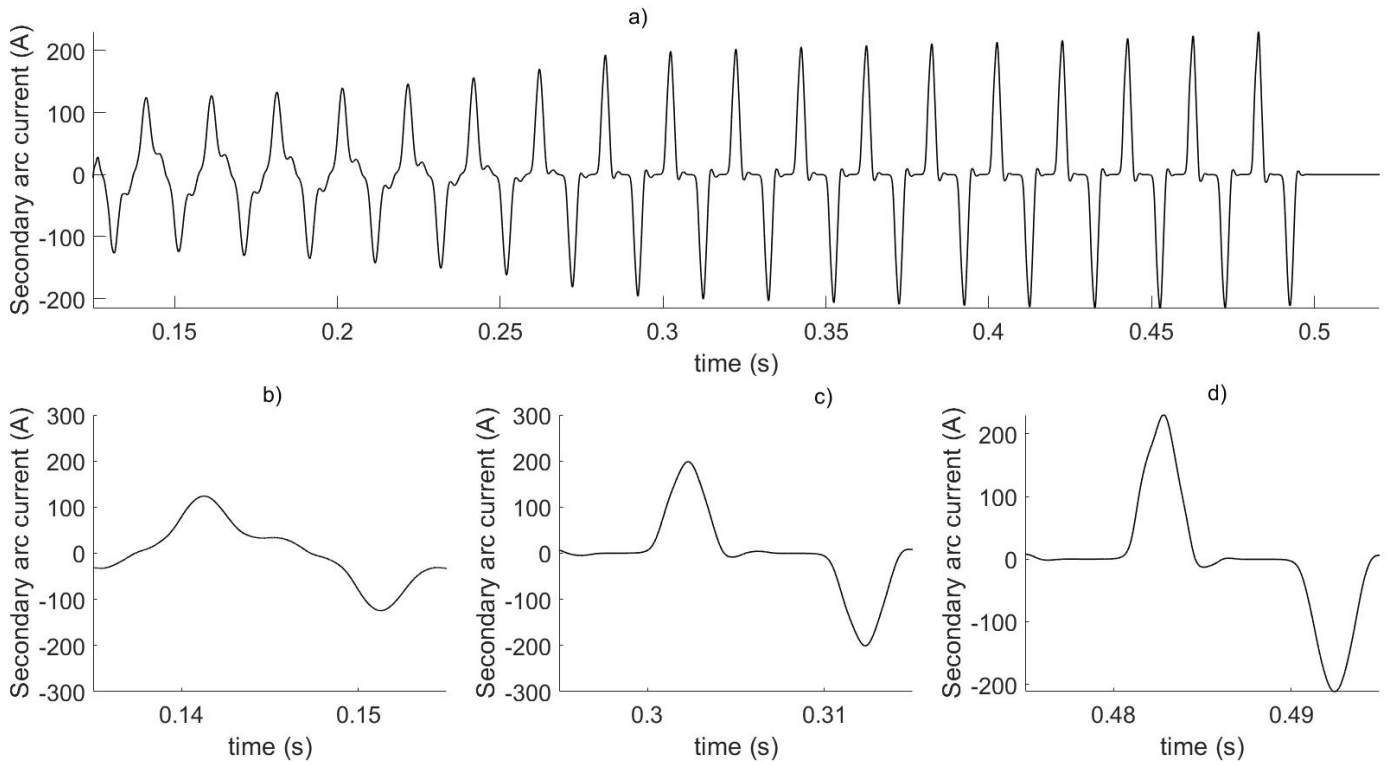


*Fig. 9 Secondary arc current vs. time (mixed line, steel ground wires, 1200 MW pre-fault loading, $v_{arc}$ = 30 m/s, fault simulated at x = 193.9 km): a) complete waveform; b, c, d) details relative to different time intervals.*
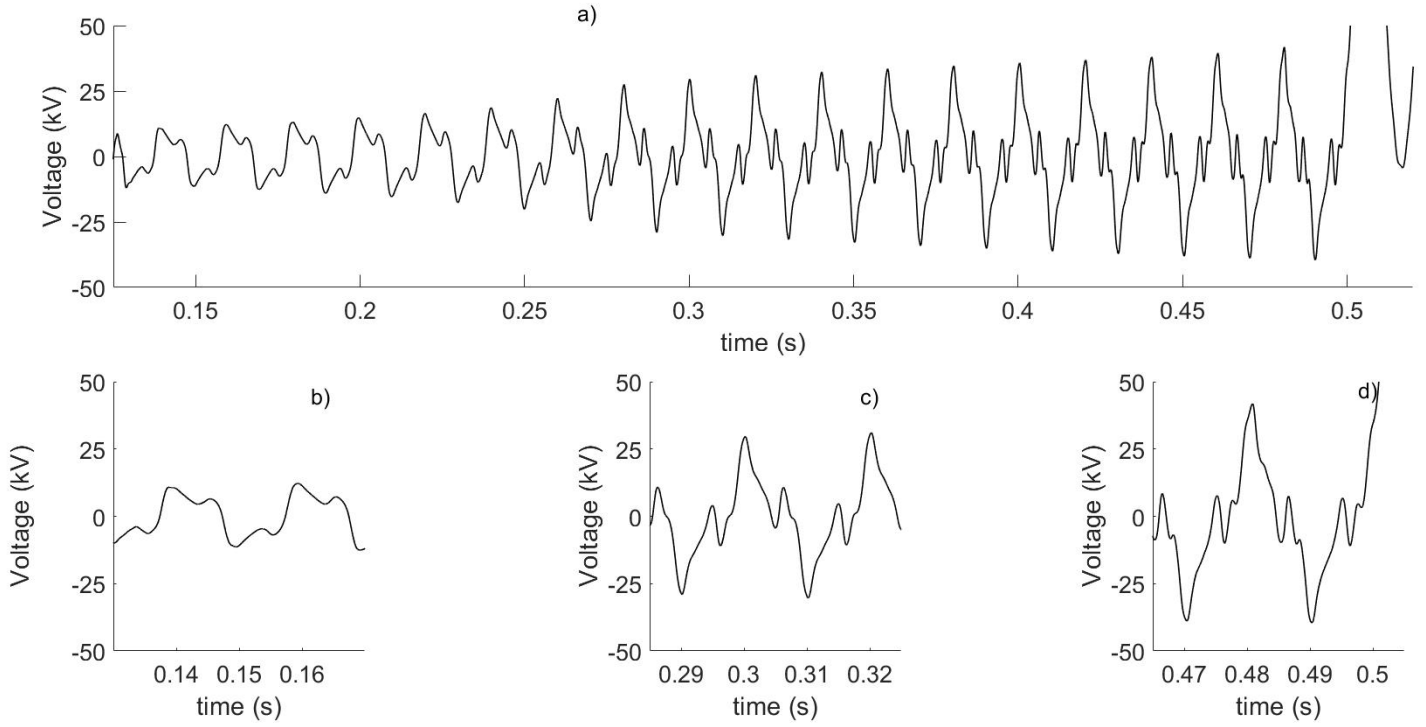
*Fig. 10 Phase-to-ground voltage vs. time (mixed line, steel ground wires, 1200 MW pre-fault loading, $v_{arc}$ = 30 m/s, fault simulated at x = 193.9 km): a) complete waveforms, b), c), d) details relative to different time intervals.*
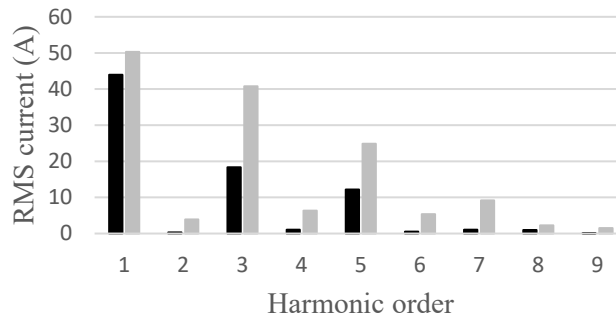


*Fig. 11 Harmonic component magnitudes of secondary arc current, for a fault occurring at x=129.3 km, recorded for the first (black) and last (grey) cycles after single-pole tripping. Mixed line, ACSR shield wires, 1200 MW pre-fault line loading.*

In both cases the harmonic content essentially consists of low-order odd harmonics (3$^{rd}$, 5$^{th}$, 7$^{th}$), but the total harmonic distortion (THD) increases from 52% to 106% before self-extinction, whereas the fundamental component of the secondary arc current only increases by 14%. Current harmonics tend to be greater for faults occurring near the cable stretch, since the large capacitance to ground of the cable offers a low-impedance path to high-frequency current components; on the other hand, the fundamental 50 Hz component is greater for faults near the sending end, as stated in [40] and shown in Fig. 8. Actually, a slight magnitude decrease of the power frequency component with time can be observed for OHL-only simulations. The increase of the power frequency component and of the overall RMS value of the secondary arc current is visualized for different parameter combinations and fault locations, in Fig. 12 and, respectively, Fig. 13.
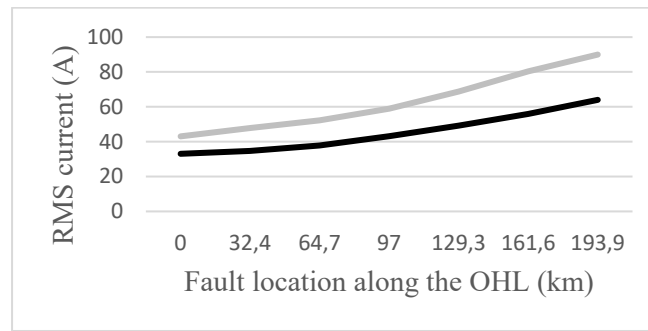


*Fig. 12 Total secondary RMS arc current values, measured in the first (black) and last (grey) cycle after single-pole tripping, for various fault locations. Mixed line, galvanized steel shield wires, 1200 MW pre-fault line loading, v$_{arc}$=30 m/s.*
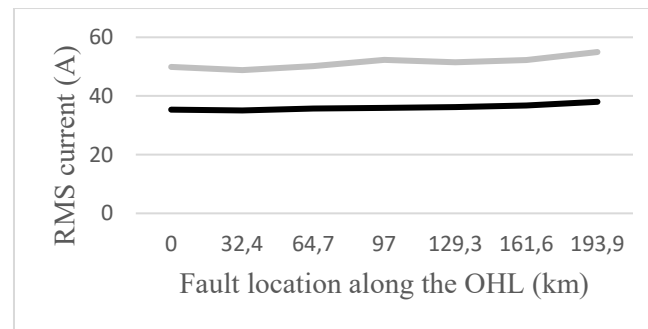


*Fig. 13 Total secondary RMS arc current values, measured in the first (black) and last (grey) cycle after single-pole tripping, for various fault locations. OHL line, ACSR shield wires, 400 MW pre-fault line loading, v$_{arc}$=30 m/s.*

## 4.3 Extinction times

The assessment of secondary arc self-extinction is the main aim of the ATP-EMTP time-domain study since it determines SPAR success. Figure 14 shows ML and OHL extinction times as a function of fault location, with an arc elongation speed $v_{arc}$ = 30 m/s, for the ACSR ground wires, and both values of pre-fault power flow (400 MW and 1200 MW).
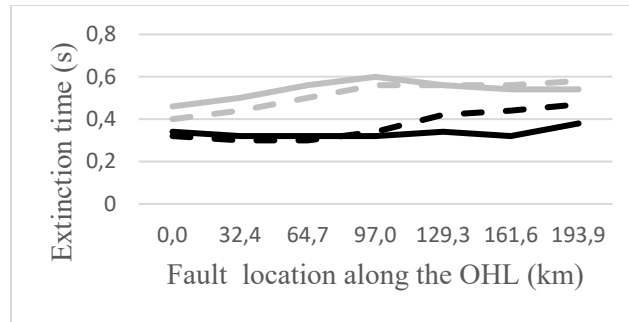


*Fig. 14 Secondary arc current extinction times vs. fault location. $v_{arc}$=30 m/s, ACSR shield wires. 400 MW (solid) vs 1200 MW (dashed) pre-fault line loading. Mixed line (black) vs OHL (grey).*

Fig. 15 shows extinction times obtained with galvanized steel ground wires, and a very conservative $v_{arc}$ = 10 m/s arc elongation speed.
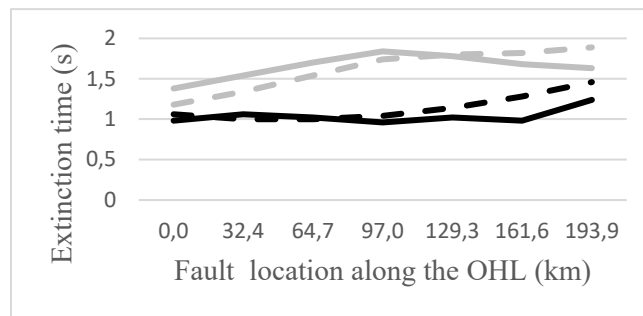


*Fig. 15 Secondary arc current extinction times vs. fault location. $v_{arc}$ = 10 m/s, galvanized steel shield wires. 400 MW (solid) vs 1200 MW (dashed) pre-fault line loading. Mixed line (black) vs OHL (grey).*

Figures 14 and 15 point out to the fact that the parameter exerting the greatest influence on extinction time is the speed of elongation $v_{arc}$: all other factors being equal, simulated extinction times are much longer with $v_{arc}$=10 m/s than with $v_{arc}$=30 m/s. A comparison between Fig. 14 and Fig. 15 shows that arc durations are roughly in an inverse proportion to the elongation speed, hinting at the fact that self-extinction occurs when

the simulated arc length reaches a given value. It is also worth of note that for a given line configuration and fault position, the secondary arc current amplitudes measured in the last cycle prior to extinction are not influenced by the assumed $v_{arc}$ value. Several of the above points are evidenced in Fig. 16, which shows the secondary arc current waveforms for faults simulated at the overhead terminal of the ML ($x$=193.9 km), relative to three different parameter combinations. Figures 16a and 16b were both obtained with steel ground wires and $v_{arc}$ = 10 m/s and differ only for the pre-fault flow (400 MW in Fig. 16a vs. 1200 MW in Fig. 16b). Figure 16.c also refer to 1200 MW pre-fault, but with ACSR shield wires and, most importantly, $v_{arc}$=30 m/s.

The most important finding from Fig. 14 and Fig. 15 is that, for any parameter combination, extinction times in the ML are shorter than in the OHL. Since extinction times obtained with the conservative but realistic value $v_{arc}$=30 m/s are not greater than 0.5 s, results point out to the applicability of SPAR to 400 kV-50 Hz uncompensated MLs.
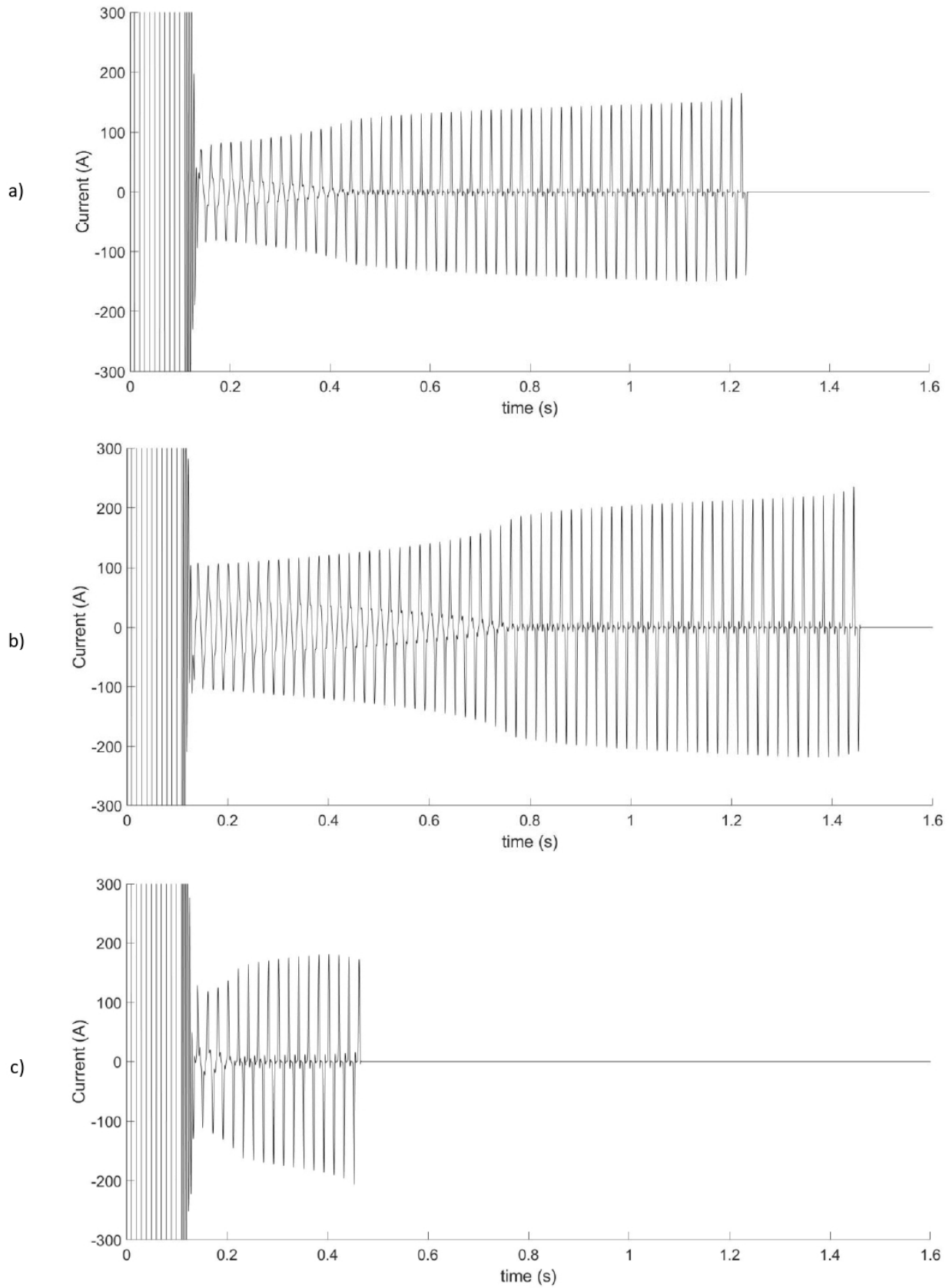
*Fig. 16 Secondary arc current vs. time, for different parameter combinations (fault simulated at x = 193.9 km).*

*a) Mixed line, pre-fault line loading 400 MW, steel ground wires, v$_{arc}$ = 10 m/s; b) mixed line, pre-fault line*

*loading 1200 MW, steel ground wires, varc = 10 m/s; c) mixed line, pre-fault line loading 1200 MW, ACSR*

*ground wires, $v_{arc}$ = 30 m/s.*

## 4.4 Recovery voltage

Figure 17 shows the faulted phase voltage to ground at fault location for the same three cases of Fig. 16. Plots encompass three distinct and successive phases, namely the primary (fault) arc voltage followed by the secondary arc voltage and lastly by the faulted phase voltage to ground after secondary arc extinction, i.e., the recovery voltage. During the recovery voltage phase, waveforms exhibit a large offset due to the trapped charge on the isolated conductor [31]. In the absence of line-connected inductive voltage transformers this slowly decaying offset amounts to a pseudo-constant voltage superimposed to the 50 Hz fundamental component: the initial peak of the recovery voltage can thus reach twice the steady-state value. Figure 18 shows the total rms recovery voltage values simulated for the ML and OHL, with 1200 MW pre-fault load, as a function of the fault location
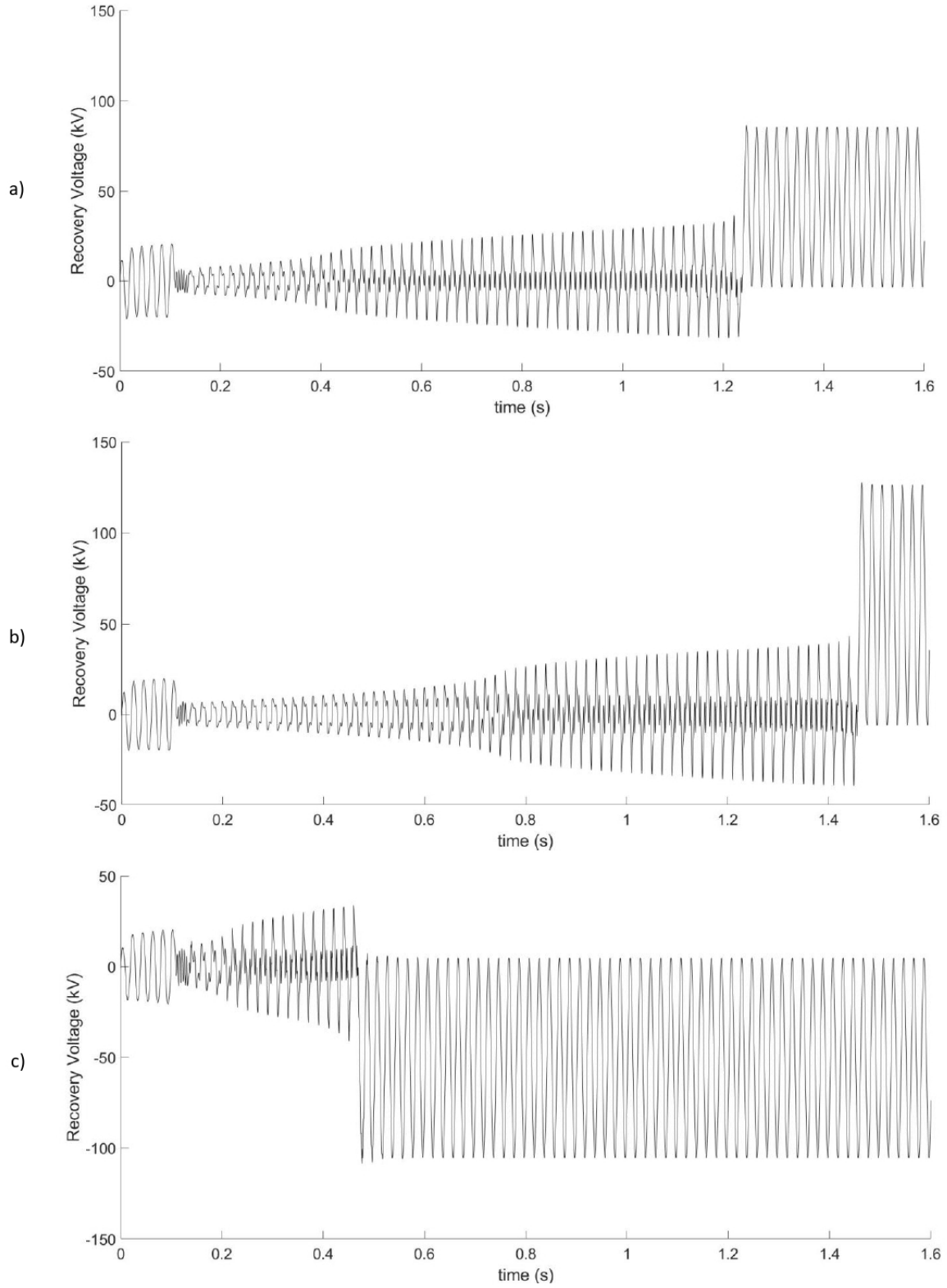
*Fig. 17 Voltage at fault location vs. time (fault simulated at x = 193.9 km). a) Mixed line, pre-fault line loading 400 MW, steel ground wires, $v_{arc}$ = 10 m/s; b) mixed line, pre-fault line loading 1200 MW, steel ground wires, $v_{arc}$ = 10 m/s; c) mixed line, pre-fault line loading 1200 MW, ACSR ground wires, $v_{arc}$ = 30 m/s.*

along the line; both the ACSR and steel shield wire cases are included. Curves in Fig. 19OLD, show the power frequency component of the recovery voltage, which follow a similar pattern and evidence a very good agreement with the steady-state values calculated in [40]. Time-domain simulations confirm that ML recovery voltages are generally smaller than those obtained for the all-overhead line, as predicted in [40]. In conjunction with the extinction times reported above, this suggests that the lower ML recovery voltage offsets the larger secondary arc current.
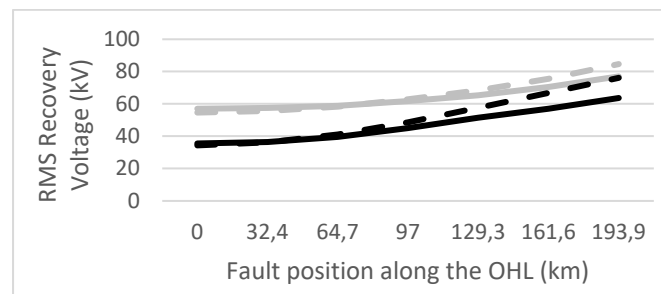


*Fig. 18 Recovery voltage – total RMS values. Calculated for various fault position, pre-fault line loading 1200 MW. ACSR (solid) vs galvanized steel (dashed) shield wires. Mixed line (black) vs OHL (grey).*
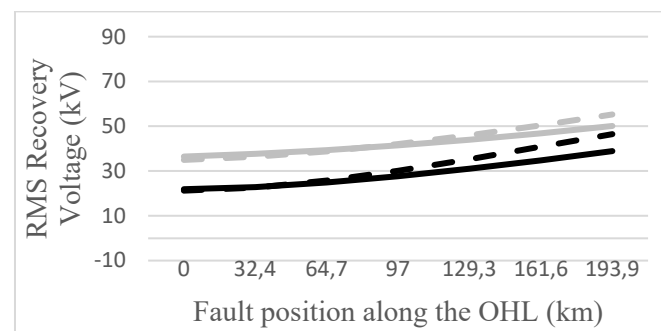


*Fig.19 Recovery voltage – Fundamental component RMS values. Calculated for various fault position, pre-fault line loading 1200 MW. ACSR (solid) vs galvanized steel (dashed) shield wires. Mixed line (black) vs OHL (grey).*

# 5 Conclusions

The single-phase autoreclosure of an uncompensated 400 kV–50 Hz overhead-cable mixed line including a short cable stretch has been investigated by means of time-domain simulations. The simulated configuration, a 201.1 km-long line consisting of 6.7 km of underground cable and 194.4 km of overhead line, was chosen due to its liability to large secondary arc currents, well in excess of the usual empirical arc self-extinction thresholds. A detailed ATP-EMTP model including dynamic modeling of the "primary" and "secondary" arc was set up, and a parametric study was carried out, varying the single-phase to ground fault location along the overhead line stretch, as well as the pre-fault line loading and the shield wire composition (for the OHL section). By way of comparison, the same cases have been simulated considering the line entirely overhead, with the same total length.

The aim of this work was firstly to validate analytical predictions from [40] and secondly to assess their impact on the secondary arc extinction time. Main findings can be summarized as follows:

- the power frequency components of both secondary arc current and recovery voltage transient waveforms are in very good agreement with previous steady-state phasor studies by the authors, confirming the increase of the secondary arc current and the concurrent decrease of the subsequent recovery voltage in the ML, compared to an overhead line;
- in transient simulations, the largest secondary arc currents are found for high pre-fault power flows going from the OHL to the CL section, and faults close to the OH terminal of the ML. Maximum currents are larger with steel, instead than ACSR shield wires;
- for a conservative 30 m/s arc elongation speed, ML secondary arc self-extinction always occurs within 0.45 s, even considering an extremely low 10 m/s elongation speed, the arc self-extinguishes within 1.4 s;
- for any given parameter combination, simulated secondary arc extinction times are always shorter for the ML than for the OHL.

The obtained arc extinction times point out to the applicability of SPAR to 400 kV-50 Hz uncompensated mixed lines. Further studies are underway, focusing on the influence of system power swings initiated by the fault as well as on the possible harmonic interaction between the line and the non-linear arc impedance.

# 6 References

[1]  R. Rendina, A. Posati, M. Rebolini, G. Bruno, F. Bocchi, M. Marelli, A. Orini, «The new Turbigo – Rho 380 kV transmission line» *Proc. CIGRE General Session*, 2006, Paper B1-302.

[2]  C. Jensen, P. Argot, «400 kV underground cables in rural areas» *Proc. CIGRE General Session*, 2006, Paper B1-211.

[3]  *ENTSOE – Europacable Joint Paper, Feasibility and technical aspects of partial undergrounding of extra – high voltage power transmission lines*, December 2010

www.ec.europa.eu/energy/infrastructure/tente/doc/offshorewind/2010annualreportannex7en.pdf.

[4]  IEEE Committee Report, «Single phase tripping and autoreclosing of transmission lines» *IEEE Trans. Power Del.* 7 (1) (1992) 182–192.

[5]  H.J. Haubrick, G. Hosemann, R. Thomas, «Single-phase auto-reclosing in EHV systems» *Proc. CIGRE General Session*, 1974, Paper 31-09.

[6]  D. E. Perry, R. M. Hasibar, J. W. Chadwick, B. J. Ware, A. J. Fakheri, R. S. Bayless, «Investigation and evaluation of single-phase switching on EHV networks in the United States» *Proc. CIGRE General Session*, 1984, Paper 39-08.

[7]  G. Ushio, K. Kurosawa, E. Itakura, W. Taki, Y. Kawasaki, M. Shintani, «Fault Detection Systems for Hybrid Line/Cable Circuits in Japan» *Paper 205 - Study Committee B5 Colloquium September 12-17, 2011, Lausanne, Switzerland*.

[8]  J. Shen, X. Zhu, Y. Li, Q. Zhao, G. Liu, D. Liu, «A New type reactance relay and Reclosing Scheme for Hybrid lines» *Paper 201 - Study Committee B5 Colloquium September 12-17, 2011, Lausanne, Switzerland*.

[9] P. Eguia, I. Zamora, A. Etxegarai, R. Cimadevilla, R. Quintanilla, « Synchrophasor based Fault Location Algorithm for Hybrid line/cable Circuits» Paper 204 - Study Committee B5 Colloquium September 12-17, 2011, Lausanne, Switzerland.

[10] CIGRÉ WG B5.23, "Short Circuit Protection of Circuits with Mixed Conductor Technologies in Transmission Networks," CIGRÉ Technical brochure 587, June 2014.

[11] K. M. C. Dantas, F. V. Lopes, K. M. Silva, F. B. Costa and N. S. S. Ribeiro, "Phasor-Based Single-Phase Auto-Reclosing Scheme for Non-Compensated Transmission Lines," in IEEE Transactions on Power Delivery, vol. 37, no. 1, pp. 219-229, Feb. 2022.

[12] M. Saad, C. -H. Kim and N. Munir, "Single-Phase Auto-Reclosing Scheme using Particle Filter and Convolutional Neural Network," in IEEE Transactions on Power Delivery.

[13] R. B. Shipley, H. J. Holley and D. W. Coleman, "Digital Analysis of Single-Pole Switching on EHV Lines," in IEEE Transactions on Power Apparatus and Systems, vol. PAS-87, no. 8, pp. 1679-1687, Aug. 1968.

[14] Farouk A.M. Rizk, «Single-phase autoreclosure of extra-high-voltage transmission lines» *PROC. IEE, Vol. 116, No. 1, 1969*.

[15] K. Anjo, H. Terase, Y. Kawaguchi, «Self-extintion of arcs created in long air gaps» *Elec. Eng. Jpn., vol. 88, pp. 83-93, 1968*.

[16] A. Balossi, M. Malaguti, P. Ostano, «Laboratory full-scale tests for the determination of the secondary arc extinction time in high-speed reclosing» *IEEE Summer Power Meeting, New Orleans, La., July 10-15, 1966.*

[17] S. B. C. Alessandra, A. A. G. Ricardo, G. R. Marcelo, F. O. Oliveira, M. P. Carlos and T. M. Cristina, "Single-phase auto-reclosure studies: secondary arc model research including a 500kV line experimental circuit," *2008 International Conference on High Voltage Engineering and Application, 2008, pp. 490-493*

[18] H. Liu, R. Li, D. He, J. Wei and Q. Li, "Experimental Study of Multiple-Reignition Features of Secondary Arcs on EHV/UHV Transmission Lines," in IEEE Transactions on Industrial Electronics, vol. 66, no. 4, pp. 3247-3255, April 2019.

[19] T. Tsuboi, J. Takami, S. Okabe, K. Aoki and Y. Yamagata, "Study on a field data of secondary arc extinction time for large-sized transmission lines," in IEEE Transactions on Dielectrics and Electrical Insulation, vol. 20, no. 6, pp. 2277-2286, December 2013.

[20] M. C. Tavares, J. Talaisys and A. Camara, "Voltage harmonic content of long artificially generated electrical arc in out-door experiment at 500 kV towers," in IEEE Transactions on Dielectrics and Electrical Insulation, vol. 21, no. 3, pp. 1005-1014, June 2014.

[21] G. Ban, L. Prikler and G. Banfai, "Testing EHV secondary arcs," 2001 IEEE Porto Power Tech Proceedings (Cat. No.01EX502), 2001, pp. 6 pp. vol.4.

[22] Y. Goda, S. Matsuda, T. Inaba and Y. Ozaki, "Forced extinction characteristics of secondary arc on UHV (1000 kV class) transmission lines," in IEEE Transactions on Power Delivery, vol. 8, no. 3, pp. 1322-1330, July 1993.

[23] A. J. Fakheri, T. C. Shuter, J. M. Schneider and C. H. Shih, "Single Phase Switching Tests on the AEP 765 KV System-Extinction Time for Large Secondary Arc Currents," in IEEE Power Engineering Review, vol. PER-3, no. 8, pp. 57-57, Aug. 1983.

[24] L. Carlsson, L. Groza, A. Cristovici, D. S. Necsulescu, A. Ionescu, "Single-Pole Reclosing on Ehv Lines". *Int Conf on Large High-Voltage Electr Syst*, CIGRE, 1974.

[25] A. Grutz, A. Hochrainer, «Rechnerische untersuchung von leistungsschaltern mit Hilfe einer verallgemeinerten Lichtbogentheorie» ETZ-A Elektrotech. Z. 92, 1971, No. 4, Pag. 185-191.

[26] M. Kizilcay, T. Pniok, «Digital Simulation of Fault Arcs in Power Systems» ETEP Journal, vol. 1, n. 1, pp. 55-60, 1991.

[27] A. Johns, R. Aggarwal, Y. Song, «Improved techniques for modelling fault arcs on faulted EHV transmission systems» IEE Proc.-Gener. Transm. Distrib., vol. 141, n. 2, pp. 148-154, 1994.

[28] M. Kizilcay, G. Ban, L. Prikler and P. Handl, "Interaction of the secondary arc with the transmission system during single-phase autoreclosure," 2003 IEEE Bologna Power Tech Conference Proceedings, 2003, pp. 7 pp. Vol.2.

[29]B. Khodabakhchian, "EHV single-pole switching: It is not only a matter of secondary arc extinction" International Conference on Power System Transients (IPST2013) in Vancouver, Canada July 18-20, 2013.

[30]L. Prikler, M. Kizilcay, G. Bàn, P. Handl, «Modelling secondary arc based on identification of arc parameters from staged fault test records» Electrical Power and Energy System, n. 25, pp. 581-589, 2003.

[31]E.W. Kimbark «Suppression of Ground-Fault Arcs on Single-Pole Switched EHV Lines by Shunt Reactors» IEEE Trans. Power Apparatus and Systems, vol. 83, pp.285-290, March 1964.

[32]O. Dias, F. Magrin and M. C. Tavares, "Comparison of secondary arcs for reclosing applications," in IEEE Transactions on Dielectrics and Electrical Insulation, vol. 24, no. 3, pp. 1592-1599, June 2017.

[33]I. Dudurych, T. Gallagher and E. Rosolowski, "Arc effect on single-phase reclosing time of an UHV power transmission line," IEEE Power Engineering Society General Meeting, 2004., 2004, pp. 581 Vol.1.

[34]Q. Sun, Z. Xiao, H. Liu, Q. Li and F. Wang, "A Study on the Transient of Secondary Arc Current of UHV Transmission Lines," in IEEE Access, vol. 6, pp. 38616-38626, 2018.

[35]M. Tavares and C. Portela, "Transmission system parameters optimization - sensitivity analysis of secondary arc current and recovery voltage," IEEE Power Engineering Society General Meeting, 2004., 2004, pp. 410 Vol.1.

[36]Jhair S. Acosta, Maria C. Tavares, Aniruddha M. Gole, "Optimizing multi-circuit transmission lines for single-phase auto-reclosing," Electric Power Systems Research, Volume 197, 2021.

[37]J. S. Acosta, M. C. Tavares and A. M. Gole, "Neutral Reactor Structures for Improved Single Phase Auto Reclosing in Multi-Circuit Multi-Voltage Transmission Lines," in IEEE Transactions on Power Delivery, vol. 37, no. 1, pp. 298-307, Feb. 2022.

[38]M. R. Dadash Zadeh, M. Sanaye-Pasand and A. Kadivar, "Investigation of Neutral Reactor Performance in Reducing Secondary Arc Current," in IEEE Transactions on Power Delivery, vol. 23, no. 4, pp. 2472-2479, Oct. 2008.

[39] Q. Ma, B. Zheng, L. Ban and Z. Xiang, "Secondary Arc Current Analysis of an Untransposed EHV/UHV Transmission Line With Controllable Unbalanced Shunt Reactor," in IEEE Transactions on Power Delivery, vol. 30, no. 3, pp. 1458-1466, June 2015.

[40] F. Gatta, A. Geri, S. Lauria, M. Maccioni, «Power frequency secondary arc current in uncompensated EHV AC mixed cable-overhead lines» *Electric Power Systems Research*, pp. 14-21, 2014.

[41] A. Mackow, M. Kizilcay, «Simulation of Secondary Arc on 400-kV Transmission System Consisting of Overhead Line Section and Power Cable Section» EEEIC, 2013.

[42] L. Colla, F. M. Gatta, F. Iliceto, S. Lauria, "Design and Operation of EHV Transmission Lines Including Long Insulated Cable and Overhead Sections," in Proc. IEEE St. Petersburg Power Tech Conf., 2005, Paper TM-3.6.